International Journal of Chemical, Materials and Biomolecular Sciences
ISSN: 2415-6620
Vol:12, No:9, 2018

Mechanical Investigation Approach to Optimize the High-Velocity Oxygen Fuel Fe-Based Amorphous Coatings Reinforced by B_4C Nanoparticles

Behrooz Movahedi

***Abstract*—**Fe-based amorphous feedstock powders are used as the matrix into which various ratios of hard B4C nanoparticles (0, 5, 10, 15, 20 vol.%) as reinforcing agents were prepared using a planetary high-energy mechanical milling. The ball-milled nanocomposite feedstock powders were also sprayed by means of high-velocity oxygen fuel (HVOF) technique. The characteristics of the powder particles and the prepared coating depending on their microstructures and nanohardness were examined in detail using nanoindentation tester. The results showed that the formation of the Fe-based amorphous phase was noticed over the course of high-energy ball milling. It is interesting to note that the nanocomposite coating is divided into two regions, namely, a full amorphous phase region and homogeneous dispersion of B4C nanoparticles with a scale of 10–50 nm in a residual amorphous matrix. As the B4C content increases, the nanohardness of the composite coatings increases, but the fracture toughness begins to decrease at the B4C content higher than 20 vol.%. The optimal mechanical properties are obtained with 15 vol.% B4C due to the suitable content and uniform distribution of nanoparticles. Consequently, the changes in mechanical properties of the coatings were attributed to the changes in the brittle to ductile transition by adding B4C nanoparticles.

***Keywords*—**Fe-based amorphous, B4C nanoparticles, nanocomposite coating, HVOF.

I. Introduction

FE-BASED metallic glasses indicate that it is a multicomponent alloy constituted of metal and metalloid elements [1]. This amorphous structure of metallic glasses gives them many unique properties compared to the crystalline materials and show the great candidates for the applications in aggressive environmental conditions including high wear and corrosion such as in ships, power stations, mines, and the machinery [2]-[4]. However, poor wear resistance in dry environments and very poor ductility significantly limit their range of possible applications as engineering and structural materials [1], [5], [6]. Furthermore, Fe-based bulk metallic glasses (BMG) always demonstrate no plastic deformation after yielding and no work hardening during the room temperature deformation due to the formation of highly localized shear bands [7]. It was found in the earlier study that Fe-based metallic glass coatings exhibited a very low-friction coefficient in a lubricating oil environment but a high-friction coefficient in a dry one. Therefore, such coatings were relatively poor in protecting against wear [8]. Although, considerable efforts have been devoted during the last decade to improve their plasticity by composition designing and developing BMG composites [2], [6].

Interestingly, reinforcement of the secondary phases (particles or crystalline phase) in the glass matrix microstructure is one of the approaches to overcome these drawbacks [8]-[10]. The addition of fine second-phase particles such as WC, B_4C or TiN in BMG composites often improves wear resistance and mechanical properties because these particles effectively block the propagation of the shear bands [11], [12]. Suh et al. [13] claimed that multi wall carbon nanotubes with a high aspect ratio and a strong bonding character of the matrix have a great role in reinforcing the Fe-based composites. Terajima et al. [8] reported that the addition of 8 vol.% WC/12 wt.%Co to the Fe-Cr-Mo-C-B matrix increased the cross-sectional hardness from 6.47 to 8.53 GPa and reduced the friction coefficient from 0.65 to 0.5. These composite coatings showed an improved wear resistance by a factor of 2–5 as compared to the single-phase amorphous coating [8], [9], [14], [15].

Boron carbide (B_4C) with many unique properties such as a high hardness (9.3 Mohs scale), high melting point 2723 K (2450 ^{o}C), excellent thermal stability, remarkable chemical inertness, and high-abrasion resistance, is extremely appropriate for moderate and high temperature applications [16]. Yoon et al. [17] reported that the friction coefficient of Fe-based BMG/B_4C composite coating (using nitrogen-shrouded plasma spraying system) was dependent on the fraction of B_4C in the BMG matrix. The wear behavior of Fe-based BMG was controlled by plastic deformation and fracture of the wear surface. By embedding a harder material, B_4C, in a relatively soft matrix, the hardness of the wear surface can be increased and the plastic flow can be inhibited.

Usually, thermal spraying technique is feasible to producing thick coatings consisting of amorphous phase since it allows rapid quenching of molten particles (around 10^5–10^7 K s^{-1}) [18]-[20]. The large amounts of work have been done on depositing amorphous metallic coatings using various thermal spraying processes. Recently, studies of Fe-based metallic glass coatings applied by the HVOF and some other thermal spraying process have been appeared in the literature [21]-[23]. These reports presented that the Fe-based metallic glass coating remains amorphous after the spraying. The HVOF technique was studied because of its ability to produce high-density coatings and improved metallurgical bonding to

Behrooz Movahedi is with the Department of Nanotechnology Engineering, Faculty of Advanced Sciences and Technologies, University of Isfahan, Isfahan, 81746-73441, Iran (e-mail: b.movahedi@ast.ui.ac.ir).

the substrate [15]. Another feature is that the process temperature can be controlled in the close range of the glass transition temperatures of metallic glasses as reported in the previous studies [8], [9], [21], [24]. A mechanism which can explain the high-hardness observed due to the formation of an amorphous/nanocrystalline composite structure has been extensively discussed [25].

According to our previous studies [22], [24], [26], [27], the as-sprayed (Fe-Cr-Mo-Mn-W-B-C-Si) coating was of almost amorphous phase and this structure had a good thermal stability. To the best of my knowledge, the effects of B_4C reinforcing nanoparticles on the microstructures and mechanical properties of the Fe-based metallic glass HVOF coatings have not been studied systematically. Thus, one of the motivations for adding the second phase particles in the amorphous matrix was to prevent the propagation of the shear bands. It is known that the brittleness of Fe-based BMG limits the engineering applications and considerable efforts have been made to improve it by introducing a composite structure. Mainly, the aims of this study are focused on the microstructure, nanohardness and toughness, of the modified Fe-based metallic glass HVOF coating reinforced by B_4C nanoparticles. Hence, the effects of B_4C content were investigated in detail with an emphasis on the characterization and nanoindentation approach.

II. Experimental Procedure

A. Feedstock Powder and Coating Preparation

The feedstock nanocomposite Fe-based metallic glass powder was prepared in the planetary high-energy ball mill in an argon gas atmosphere. The elemental powders were blended to give a nominal composition of (Fe-15%Cr-2%Mo-4%Mn-4%W-5%B-0.5%C-1%Si) with various amounts of B_4C nanoparticles (0, 5, 10,15, 20, 25%, all in volume percent). Fe, Cr, W, B powders (purity: 99.0%, mean particle size: +100 μm), Mo, Mn, Si, C powders (purity: 99.5%, mean particle size: -50 μm) and B_4C (purity: 99.0%, mean particle size: 45-55 nm, US-Research Nanomaterials Inc.) were used as the starting materials. The details of the feedstock glassy powder fabrication were reported elsewhere [26], [27]. It is doubtful, whether the embedding of the B_4C nanosized powders between the elemental layers during the mechanical alloying process could delay the formation of amorphous structure. On the other hand, the B_4C nanoparticles hinder the cold welding and the fracturing process during mechanical alloying, and thus, the refining of layer thickness cannot move forward. Thus, in the current work, following the formation of amorphous phase, the B_4C nanoparticles was added to the amorphous powder mixture for fabricating nanocomposite powders [28].

HVOF spraying was performed using Metallization Met JET III system. The modified spraying conditions have been summarized in Table I. The mild steel (BS080A15) substrate (50×50×5mm) surfaces were cleaned prior to spraying by sand-blast with alumina grit on the one side followed by ultrasonic cleaning in acetone to remove any contaminations. The substrates were mounted on a vertical axis of a turntable, and the rotation speed was set to impart a surface velocity to the substrates of approximately 1.1 m/s across the spray path. The HVOF gun was positioned in front of them, aligned to give a spray path perpendicular to the axis and set to the required stand-off from the surface of the substrates. It was then scanned vertically up and down at 10 mm/s to build up a coating of the required thickness. To avoid significant heating during the progress of the process and maintain the substrate temperature below 473K (200° C), the substrates were cooled on their backside using compressed argon gas.

TABLE I
HVOF Spraying Parameters for Fe-Based Metallic Glass Coating

Parameter	Value
O_2 gas flow rate (SLPM*)	833
Fuel (Kerosene) flow rate (SLPM)	0.37
Nozzle length (mm)	100
Powder feed rate (g/min)	35
Stand-off distance (mm)	300
Scanning velocity (mm/s)	10
Coating thickness (μm)	320-380
Cooling (Argon gas)	yes

*SLPM: Standard liter per minute

B. Characterization Techniques

X-ray diffraction (XRD: Philips XPERT-MPD) was performed to study the structural evolutions. All XRD experiments were carried out in the continuous scanning mode using Cu-K_α radiation (λ=0.1542 nm), time per step of one second and 0.03º step size. The cross-sectional microstructures of the coatings were investigated using scanning electron microscopy (SEM: JEOL JSM-6360A). High-resolution transmission electron microscopy (HRTEM) was performed using JEOL-JEM-2010 TEM at an accelerating voltage of 200 kV and resolution of 0.19 nm. To prepare the sample, the coating was first sectioned with a diamond saw and then mechanically thinned to about 100 μm with emery paper. In the second step, the thickness of the thinned layer was decreased down to 5 μm using a dimpling machine (Gatan dimple grinder 656). The final step was ion-milling at a low incident angle (Gatan ion polishing 691) to obtain a very thin layer of less than 100 nm.

C. Mechanical Investigation Tests

The indentation experiments were carried out on the polished surface of the coatings at room temperature using a commercial nanoindenter (CSM Instruments SA, Peseux, Switzerland) with a Berkovich tip (a few tens of nanometers in diameter). In the load schedules employed, the load at the constant rate was first ramped up to a peak value of 10 mN and then unloading. Each test was performed three times, and the average was reported.

The fracture toughness of HVOF coatings was determined by the indentation method. A Vickers indenter (Matsuzawa MAXT70) was used on metallographically prepared cross-sections of coatings with a 20-N load. The indenter was positioned such that the two indent diagonals were parallel and perpendicular to the substrate/coating interface,

respectively. Following the indentation, no cracking was seen in the plane perpendicular to the coating/substrate interface, but was, generally, though not always, seen to be parallel to the coating/substrate interface. The lengths of the latter cracks were measured from scanning electron micrographs imaged in the secondary electrons (SE) mode. At least 20 indentations from each coating were examined. The fracture toughness (K_c) values were calculated using cracks parallel to the substrate/coating interface. The equation for the indentation fracture toughness has been selected for the work due to its applicability to systems generating short cracks as given by Evans and Wilshaw [29] is:

$$K_c=0.079(P/a^{3/2}) Log (4.5a/c) \quad (1)$$

where P is the applied indentation load (N); a, the indentation half diagonal (m) and c the crack length from the center of the indent (m). The recommended c/a ratio for use in this equation is $0.6 \leq c/a < 4.5$.

III. Results and Discussion

A. Nanoindentation Approach

Typical load versus depth of penetration (P-h) curves obtained from the nanoindentation tests on the metallic glass coatings with different B_4C content are shown in Fig. 1. The maximum load (P_{max}) is 10 mN. The results on nanohardness (H), elastic modulus (E), H/E ratio, the maximum displacement of the nanoindenter (h_{max}), final indentation depth (h_f), h_f/h_{max} ratio, and the percentage elastic recovery of displacement on unloading $R\%=[(h_{max}-h_f)/h_{max})\times100]$ for the single-phase amorphous coatings, and reinforced with various ratios of B_4C nanoparticles are summarized in Table II.

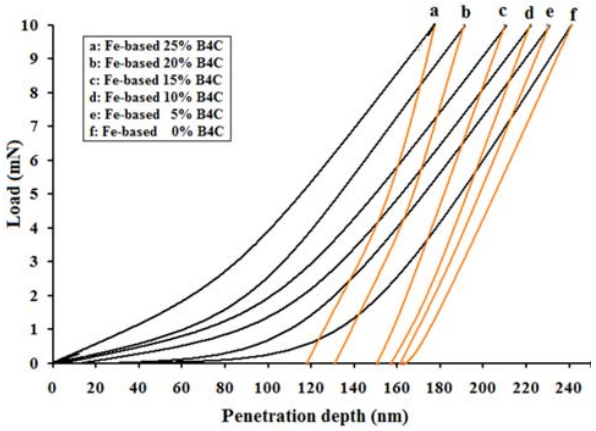

Fig. 1 Typical load versus depth of penetration (P-h) curves for the metallic glass coatings with different B_4C content

TABLE II
Summary of Nanoindention Testing and Mechanical Properties of Fe-Based Metallic Glass HVOF Coatings with Various B4C Nanoparticles

Coating compositions (vol%)	H GPa	E GPa	K_c (MPa√m)	H/E	h_f (nm)	h_{max} (nm)	h_f/h_{max}	R%
0% B_4C	8.1	133	3.0	0.061	163.3	241.2	0.677	32.30
5% B_4C	9.8	161	4.1	0.061	162.1	230.1	0.704	29.55
10% B_4C	10.3	169	4.8	0.061	157.2	222.1	0.708	29.22
15% B_4C	11.6	181	5.5	0.064	151.2	210.1	0.720	28.03
20% B_4C	12.2	185	2.8	0.066	131.1	191.3	0.685	31.47
25% B_4C	13.1	202	2.1	0.065	118.3	177.1	0.668	33.20

The nanohardness and elastic modulus of the coatings can be calculated from the curves in Fig. 1. It is evident that the maximum penetration depth (h_{max}) which is decreased by raising the amount of B_4C content in the amorphous matrix probably indicates a higher hardness appeared in the reinforced coatings. The measured hardness of the single-phase amorphous coating is 8.1 GPa, while it is 13.1 GPa for coating with 25 vol.% B_4C. The higher hardness of the latter is probably associated with a high amount of nanoparticles distributed in the amorphous matrix. The reported hardness values here are slightly higher than those measured by conventional microindenters probably because of the indenter size effect at small load levels.

Branagan et al. [30] reported that the hardness of the plasma-sprayed Fe-Cr-Mo-B-C-Si-Al coating is 10.7 GPa. Cheng et al. [23] reported that the hardness of the Fe-B-Si-Cr-Nb-Mn-Y amorphous/nanocrystalline coating is around 8.83-10.3 GPa. According to Salahinejad et al. [31], the hardness of the 78Fe-18Cr-4Mn alloy is at a maximum when the material is composed of a mixture of crystalline nanoparticles and an amorphous phase. It was explained that the amorphous/crystal interface had a lower interfacial energy than the crystal/crystal interface. This composite structure blocks the propagation of the shear bands and cracks. Kim et al. [32] have noted that the nanoparticles were too small to contain defects such as dislocations, stacking faults, or microtwins. Therefore, localized shear deformation in metallic glasses can effectively be suppressed by a possible interaction between shear bands and nanoparticles. Zhou et al. [33] reported that the Fe-Cr-Mo-C-B-Y amorphous coatings demonstrate high-average microhardness of 9.78 GPa. They concluded that the dispersion strengthening of nanocrystals precipitated in an amorphous matrix contributes to the high-hardness of as-deposited coatings.

Elastic moduli of the reinforced coatings are found to be higher than the single-phase amorphous coating. The enhancement in elastic modulus is due to the B_4C nanoparticles which act as hindrances to the shear band

propagation. The higher slope of the unloading curves indicates a higher stiffness or elastic modulus. It is clear that the unloading slope was increased by raising the B_4C nanoparticles. These results have been well documented in some reviews [8], [34].

The maximum value of nanohardness to the elastic modulus ratio (H/E) for the single-phase amorphous coating is about 0.061 which is comparable with that for bulk amorphous steels and many other BMGs [35]. The h_f/h_{max} ratio and R% are two important parameters that can be derived from the (P-h) curves. The limits of h_f/h_{max} are $0 \leq h_f/h_{max} \leq 1$. The lower limit corresponds to fully elastic deformation, whereas the upper limit is characteristic of rigid plastic materials [35]. The value of this ratio is found to be increased for coatings with B_4C up to 15 vol.%, and then, it was decreased for coatings with more than 20 vol.% B_4C nanoparticles. The reverse trend is shown for the percentage elastic recovery (R%) which indicates that the single-phase amorphous and reinforced coatings with a high amount of nanoparticles (20 and 25 vol.% B_4C) maybe deformed elastically. The h_f/h_{max} ratios in the present case are found to be in the range of 0.668–0.720, while the percentage elastic recovery ranges between 28.03% and 33.2%.

It is liable that the single-phase amorphous coating of the present study has a lower resistance to crack initiation (K_c=3 MPa√m). It is also possible that it can be correlated to a lower susceptibility to plastic flow (R= 32.3%). This is in agreement with other studies. Comparable toughness values for Fe-based glassy alloys have been reported either by indentation techniques, 3.2-3.8 MPa√m [36], [37].

In amorphous matrix, crack nucleation is effectively arrested, but crack propagation is enhanced, and single-phase amorphous materials are naturally very brittle under tension. Therefore, homogeneously distributed of 5-15 vol.% B_4C nanoparticles in the amorphous coatings enables providing random paths for crack propagation which consumes crack tip energy and restrain crack propagation [38]. Therefore, the fracture toughness enhances to 4.1-5.5 MPa√m. Accordingly, excessive B_4C nanoparticles (more than 20 vol%) reduce the fracture toughness of the coating and making it brittle and easy to be fractured during the indentation test.

It is well known that the optimization of the Fe-based metallic glass HVOF coatings, using a different amount of B_4C nanoparticles, plays a key role in enhancing the mechanical properties in order to obtain a nanocomposite coating with high hardness and fracture toughness. Hence, it is generally accepted that the optimum composition is Fe-based metallic glass with 15 vol% B_4C nanoparticles which will be discussed in the following sections.

B. Phase Evaluations and Microscopic Observations

Fig. 2 shows the XRD pattern of the as-sprayed HVOF coating compared to that of starting feedstock powder containing 15 vol.% B_4C in the Fe-based amorphous matrix. Evidently, a very large broad peak maximized at 2Θ of about 45° can be observed for the both coating and starting powder, although some small peaks from B_4C were superimposed. No other phases are detected within the sensitivity limits of X-ray diffraction. This implies that the presence of B_4C during spraying did not adversely affect the glass forming ability of the matrix. Apparently, the XRD results confirmed that the B_4C nanoparticles are in the amorphous matrix without causing any other phase formation and decomposition.

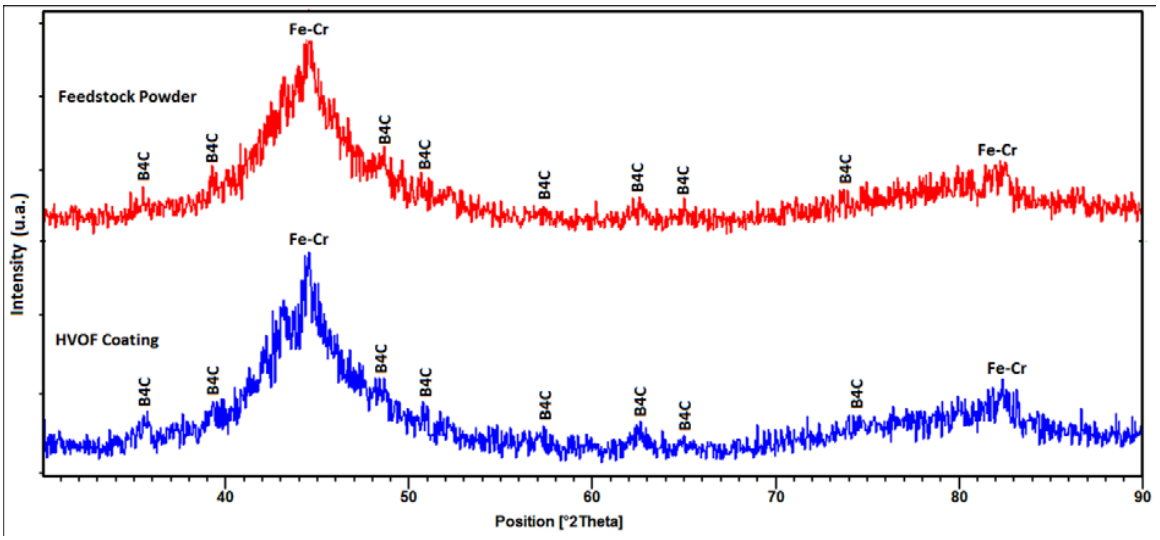

Fig. 2 XRD patterns of Fe-based-15vol.%B_4C metallic glass feedstock powder and HVOF nanocomposite coating.

TEM was undertaken to obtain more detailed information on the microstructure as shown in Fig. 3, the typical bright and dark filed TEM microstructure images of the HVOF nanocomposite coating with 15 vol.%B_4C nanoparticles. In the lattice image, Fig. 3 (a), some B_4C particles with a size of about 10-50 nm are imaged. The diffused halo Debye ring in the selected area electron diffraction pattern (SADP) confirms that the matrix regions of coating have an amorphous

structure. Furthermore, the fast Fourier transform (FFT) can be seen in the inset of Fig. 3 (b). It clearly shows the appearance of diffuse spotty patterns indicating the amorphous structure of the matrix. The dark filed image, Fig. 3 (c), validates the existence of B_4C crystals in the matrix. The HRTEM micrograph (Fig. 3 (b)) confirms the coexistence of a mixture of nanocrystalline B_4C nanoparticles within an amorphous matrix. It is interesting to point out that the diffuse characters seen in the SADP images (inset of Fig. 3 (a)) were corroborated with the XRD results noted in Fig. 2. It is evident to the HRTEM micrograph (arrow indicated in Fig. 3 (b)) that the B_4C nanoparticles are found to be homogeneously surrounded by the amorphous phase with semi-uniform interface throughout the thickness of the coating. With reference to the work of Aizenshtein et al. [39], the wetting and the interface phenomena in the (Fe–B–C)/B_4C systems are controlled by the decomposition of B_4C and the formation of an interaction zone at the ceramic/metal interface. On the other hand, a Fe-rich liquid phase is formed between the ceramic particles during thermal spraying and promoted the densification of the nanocomposite coatings.

The SEM image of the cross-section regions in the HVOF nanocomposite coating with 15 vol.%B_4C nanoparticles is shown in Fig. 4. The percentage of porosity in the coating was evaluated using image analysis (Digimizer Version 4.6.1). The values given are the average of 10 measurements. It can be seen that the coating has a highly dense and compact structure with porosity of about 0.4%±0.1 and is well bonded to the substrate with no cracking. The microstructure of HVOF coating was consisted of deformed and partially melted particles along with the fine lamellar structure. When most of the sprayed particles partially reach the melted state, only the melted fraction may form an amorphous phase, while the un-melted fraction will keep the original amorphous microstructure of the starting powder [40].

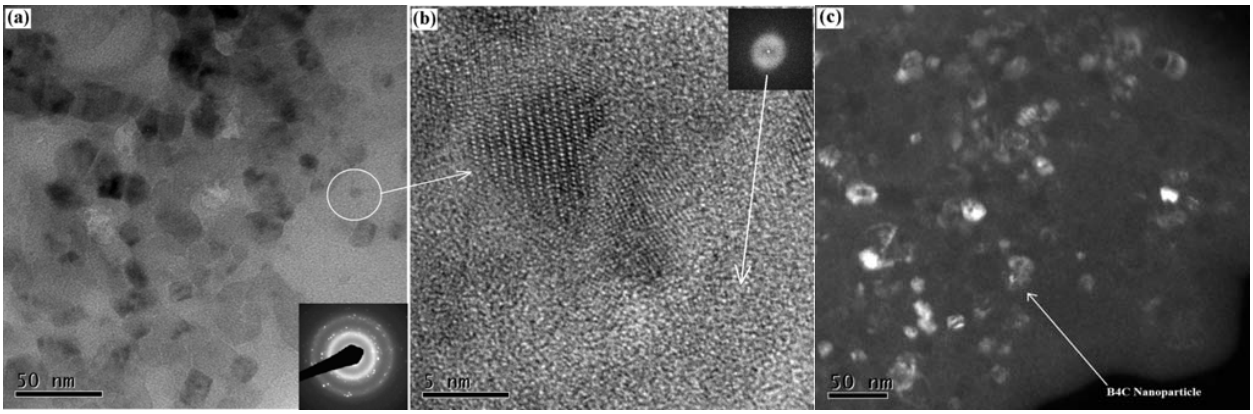

Fig. 3 (a)-(c) Bright and dark filed TEM micrographs, SADP and FFT of HVOF coating with 15 vol.%B_4C nanoparticles

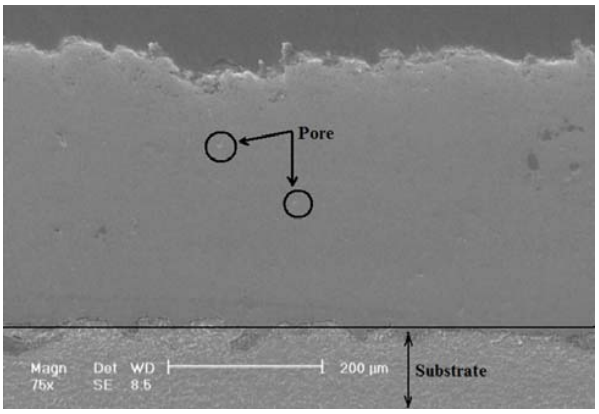

Fig. 4 SEM cross-sectional images of HVOF nanocomposite coating with 15 vol.%B_4C nanoparticles

IV. Conclusion

In the framework of this approach, the microstructural observations confirmed that the B_4C nanoparticles which act as a reinforcing agent, were well embedded in Fe-based metallic glass throughout the coating microstructures. It was observed that, with the content of B_4C nanoparticles increasing to 15 vol.%, the fracture toughness of the coatings rises from 3.0 to 5.5 MPa√m. But, when the B_4C content is higher than 20 vol.%, the fracture toughness decreases to 2.1 MPa√m. Elastic modulus as well as the h_f/h_{max} ratio was increased and the percentage elastic recovery (R%) of the coatings was gradually decreased with respect to the increase in the volume fraction of B_4C up to 15%. In the other words, the nanocomposite coating in which B_4C nanoparticles were embedded in an amorphous matrix, yielded the highest hardness compared to the single-phase amorphous coating.

References

[1] J. Do, S. Jung, H-J. Lee, B-J. Lee, G-U. Cha, C.Y. Jo and S. Lee: Metall.Tranns. A, 2013, vol. 44, pp. 2573-80.
[2] C. Zhang, L. Liu, K.C. Chan, Q. Chen and C.Y. Tang: Intermetallics, 2012, vol. 29, pp. 80-5.
[3] D. J. Branagan: Computer Coupling of Phase Diagrams and Thermochemistry 2007, vol. 31, pp. 343-50.
[4] D. J. Branagan and Y. Tang: Composites: part A, 2002, vol. 33, pp. 855-59.
[5] D. Z. Segu, J. H. Choi, S. Yi and S. S. Kim: Tribol Lett, 2012, vol. 47, pp. 131-38.
[6] S. F. Guo, L. Liu, N. Li and Y. Li: Scripta Materialia 2010, vol. 62, pp. 329-32.

[7] Suryanarayana and A. Inoue: Bulk Metallic Glasses. (Taylor and Francis Group, LLC, 2011).
[8] T. Terajima, F. Takeuchi, K. Nakata, S. Adachi, K. Nakashima and T. Igarashi: Journal of Alloys and Compounds 2010, vol. 504, pp. 288-91.
[9] S. Yugeswaran, A. Kobayashi, K. Suresh and B. Subramanian: Journal of Alloys and Compounds, 2013, vol. 551, pp. 168–75.
[10] B. Y. Fu, D. Y. He, L. D. Zhao and X. Y. Li: Surface Engineering, 2009, vol. 25, pp. 326-32.
[11] D. H. Kwon, E. S. Park, M. Y. Huh, H. J. Kim and J. C. Bae: Journal of Alloys and Compounds 2011, vol. 509S, pp. S105–S108.
[12] T. Lampke, B. Wielage, H. Pokhmurska, C. Rupprecht, S. Schuberth, R. Drehmann and F. Schreiber: Surface and Coatings Technology 2011, vol. 205, pp. 3671–76.
[13] J. Y. Suh and D. H. Bae: Materials Science and Engineering A 2013, vol. 582, pp. 321-25.
[14] H. Choi-Yim and W. L. Johnson: Appl. Phys. Lett 1997, vol. 71, pp. 3808-10.
[15] L. Liu and C. Zhang: Thin Solid Films 2014, vol. 561, pp. 70-86.
[16] Y. Cao, C. Huang, W. Liu, W. Zhang and L. Du: journal of Thermal Spray Technology 2014, vol. 23, pp. 716-24.
[17] S. Yoon, J. Kim, B.D. Kim and C. Lee: Surface and Coatings Technology 2010, vol. 205, pp. 1962–68.
[18] G. Liu, Y. A.J. Chen, G. Hou and J. Chen: Tribol Lett 2012, vol. 46, pp. 131–38.
[19] H. J. Kim, K. M. Lim, B. G. Seong and B. G. Seong: Journal of Aterials Science 2001, vol. 36, pp. 49– 54.
[20] W. Tillmann, P. S. Hollingsworth, G. Fischer, J. Nellesen and F. Beckmann: Journal of Thermal Spray Technology 2014, vol. 23, pp. 289-95.
[21] Y. Wu, P. Lin, G. Xie, J. Hu and M. Cao: Materials Science and Engineering A 2006, vol. 430, pp. 34-39.
[22] B. Movahedi, In Advanced Plasma Spray Applications, ed. Hamidreza Salimi Jazi (InTech: Janeza Trdine 9, 51000 Rijeka, Croatia, 2012), pp 189-218.
[23] J-B. Cheng, X-B. Liang, B-S. Xu and Y-X. Wu: Journal of Non-Crystalline Solids 2009, vol. 355, pp. 1673–78.
[24] B. Movahedi, M.H. Enayati and C.C. Wong, journal of Thermal Spray Technology 2010, vol. 19, pp. 1093–99.
[25] W. Guo, Y. Wu, J. Zhang, S. Hong, G. Li, G. Ying, J. Guo and Y. Qin: journal of Thermal Spray Technology 2014, vol. 23, pp. 1157-80.
[26] B. Movahedi, M.H. Enayati and C.C. Wong: Materials Letters 2010, vol. 64, pp. 1055–58.
[27] B. Movahedi, M.H. Enayati and C.C. Wong: Materials Science and Engineering B 2010, vol. 172, pp. 50–54.
[28] B. Movahedi, Advanced Powder Technology 2014, vol. 25, pp. 871–78.
[29] A. G. Evans and T. R. Wilshaw: Acta Metallurgica 1976, vol. 24, pp. 939–56.
[30] D. J. Branagan, W. D. Swank, D. C. Haggard and J. R. Fincke, Metallurgical and Materials Transactions A: 2001, vol. 32, pp. 2615-21.
[31] E. Salahinejad, R. Amini, E. A. Bajestani and M. Hadianfard: Journal of Alloys and Compounds 2010, vol. 497, pp. 369-72.
[32] Y. Kim, K. Hiraga, A. Inoue, T. Masumoto and H. Jo: Mater. Trans. JIM 1994, vol. 35, pp. 293-302.
[33] Z. Zhou, L. Wang, D. Y. He, F. C. Wang and Y. B. Liu: Journal of Thermal Spray Technology 2010, vol. 19, pp. 1287–93.
[34] K. Wang, T. Fujita, D. Pan, T. G. Nieh, A. Inoue, D. H. Kim and M. W. Chen: Acta Mater 2008, vol. 56, pp. 3077–87.
[35] M. Iqbal, J. I. Akhter, H. F. Zhang and Z. Q. Hu: Journal of Non-Crystalline Solids 2008, vol. 354, pp. 5363–67.
[36] V. Keryvin, V. H. Hoang and J. Shen: Intermetallics 2009, vol. 19, pp. 211-7.
[37] P. A. Hess, S. J. Poon, G. J. Shiflet and R. H. Dauskardt: J. Mater. Res 2005, vol. 20, pp. 783-6.
[38] B. Movahedi: Surface and Coatings Technology 2013, vol. 235, pp. 212–9.
[39] M. Aizenshtein, I. Mizrahi, N. Froumin, S. Hayun, M. P. Dariel and N. Frage: Materials Science and Engineering A 2008, vol. 495, pp. 70-4.
[40] C-J. Li, Y-Y. Wang and H. Li: J. Vac. Sci. Technol. A 2004, vol. 22, pp. 2000-04.